Equilibrium shape of core(Fe)–shell(Au) nanoparticles as a function of the metals volume ratio

Anne Ponchet, Ségolène Combettes, Patrizio Benzo, Nathalie Tarrat, Marie-José Casanove, Magali Benoit

Journal of Applied Physics

Equilibrium shape of core(Fe)–shell(Au) nanoparticles as a function of the metals volume ratio

Cite as: J. Appl. Phys. **128**, 055307 (2020); https://doi.org/10.1063/5.0014906
Submitted: 23 May 2020 • Accepted: 13 July 2020 • Published Online: 05 August 2020

A. Ponchet, S. Combettes, P. Benzo, et al.

Journal of Applied Physics ARTICLE scitation.org/journal/jap

Equilibrium shape of core(Fe)–shell(Au) nanoparticles as a function of the metals volume ratio

Cite as: J. Appl. Phys. **128**, 055307 (2020); doi: 10.1063/5.0014906
Submitted: 23 May 2020 · Accepted: 13 July 2020 ·
Published Online: 5 August 2020

A. Ponchet,[a] S. Combettes, P. Benzo, N. Tarrat, M. J. Casanove, and M. Benoit

AFFILIATIONS

CEMES-CNRS, Université de Toulouse, UPS, 29 rue Jeanne Marvig, BP 94347 Toulouse Cedex 04, France

[a]**Author to whom correspondence should be addressed:** anne.ponchet@cemes.fr

ABSTRACT

The equilibrium shape of nanoparticles is investigated to elucidate the various core–shell morphologies observed in a bimetallic system associating two immiscible metals, iron and gold, that crystallize in the bcc and fcc lattices, respectively. Fe–Au core–shell nanoparticles present a crystalline Fe core embedded in a polycrystalline Au shell, with core and shell morphologies both depending on the Au/Fe volume ratio. A model is proposed to calculate the energy of these nanoparticles as a function of the Fe volume, Au/Fe volume ratio, and the core and shell shape, using the density functional theory-computed energy densities of the metal surfaces and of the two possible Au/Fe interfaces. Three driving forces leading to equilibrium shapes were identified: the strong adhesion of Au on Fe, the minimization of the Au/Fe interface energy that promotes one of the two possible interface types, and the Au surface energy minimization that promotes a 2D–3D Stranski–Krastanov-like transition of the shell. For a low Au/Fe volume ratio, the wetting is the dominant driving force and leads to the same polyhedral shape for the core and the shell, with an octagonal section. For a large Au/Fe ratio, the surface and interface energy minimizations can act independently to form an almost cube-shaped Fe core surrounded by six Au pyramids. The experimental nanoparticle shapes are well reproduced by the model, for both low and large Au/Fe volume ratios.

I. INTRODUCTION

Bimetallic nanoparticles (NPs) can be synthesized in different shapes, sizes, and structures. For two immiscible metals, the chemical order can be core–shell, Janus, or multi-shell.[1–3] These morphologies combined to size effects are at the origin of new or exalted properties compared to monometallic NPs. Bimetallic NPs are thus widely investigated for a variety of applications including catalysis, optics, magnetic recording, hyperthermia, magnetically driven drug delivery, and bactericidal actions.[1] In the Fe–Au system, a core–shell order with iron at the core preserves the magnetic properties of the iron and protects it from oxidation thanks to the gold shell. The latter also ensured the NP biocompatibility. The preservation of the magnetic properties of the core requires controlling its crystallinity, its size, and the thickness of the protecting shell. As the adsorption of molecules depends of the crystalline orientation of gold,[4] biological applications based on molecule binding also require managing the crystalline quality and orientation of the shell facets.

Predicting the NP shapes on a rational basis is thus desirable; however, it is challenging. Although the usual concepts of the crystal growth remain relevant, such as those related to epitaxy, adhesion, or elasticity, new models are required to understand the specific geometry of core–shell NPs, which cannot be directly deduced from the structural properties of the two components in their own phase or from the growth modes on a 2D substrate. The case where both core and shell are fcc crystals was deeply investigated.[5,6] This contrasts with Fe–Au NPs, a study case where the Fe core and the Au shell crystallize, respectively, in the body-centered cubic (bcc) lattice and face-centered cubic (fcc) lattice, whereas remaining in a core–shell geometry, both core and shell morphologies of Fe–Au NPs strongly evolve as a function of the respective volumes of the two metals.[7] In this article, we aim at uncovering the mechanisms responsible for this important morphological evolution. As for some other nanostructures,[8] the continuous approach adopted here provides a theoretical frame to explore the energy landscape as a function of the core and shell morphologies for NPs of any size, particularly in the typical experimental range (from 1 to 50 nm[7,9–11]), and as such is a complementary approach to atomistic simulations.

In previous studies,[7,9] nanometric AuFe based NPs were formed at high temperature (600 °C–800 °C) in an ultrahigh vacuum growth

process by the sequential deposition of Fe and then Au. They exhibit a regular core–shell shape where Fe forms a single crystal with a polyhedral shape, entirely covered by a polycrystalline Au shell. Two morphologies are observed (in the following, we will systematically refer crystallographic notations to either Fe or Au nanocrystals).

In the NPs, such as those presented in the cross section in Fig. 1(a), the Fe core is close to a perfect ⟨001⟩Fe oriented cube, and the Au shell consists essentially in six single crystals located on the {001}Fe faces of the cube. Each of these six crystals is {001}Au oriented and is constituted by a thin wetting layer surmounted by a truncated pyramid with four {111}Au sides. The dominant interfaces are {001}Au/{001}Fe (green dashed lines in the crystallographic scheme).

In Fig. 1(b), the Fe core appears in the cross section as an octagon. The core can thus be described as a polyhedron limited by {001}Fe and {110}Fe faces. The shell has a homogeneous thickness without pyramids. Two interfaces coexist: the same {001}Au/{001}Fe interface as in Fig. 1(a), and the {111}Au/{110}Fe interface (red dashed lines in the scheme). The shell is thus formed by 18 different crystallites, 12 ⟨111⟩Au oriented on the {110}Fe faces, and 6 ⟨001⟩Au oriented on the {001}Fe faces (respectively filled in red and yellow in the scheme).

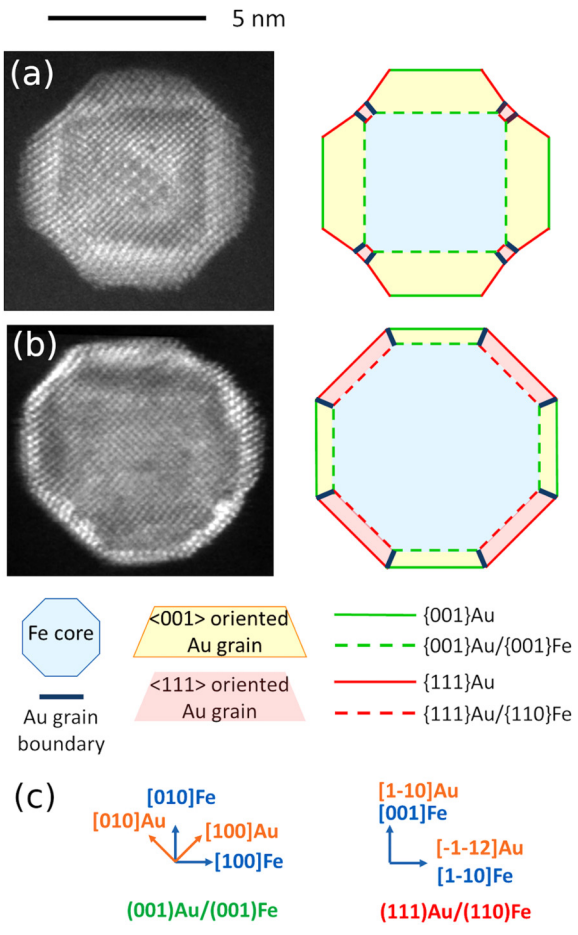

FIG. 1. Typical NPs for large (a) and small (b) shell/core volume ratio. High resolution transmission electron microscopy images (left) and corresponding crystallographic models (right). (c) In-plane epitaxial relationships for both interfaces.

The {001}Au/{001}Fe interface[7] presents a perfect epitaxial relationship thanks to a 45° rotation of {001}Au with respect to {001}Fe [Fig. 1(c)]. This orientation reduces the effective misfit to 0.6% (the lattice constant of bcc Fe and fcc Au being 0.286 65 nm and 0. 407 84 nm, respectively[12]) leading to a pseudomorphic growth of Au on Fe, without dislocations. For the {111}Au/{110}Fe interface, both theoretical[13] and experimental[14] results agree with the so-called Nishiyama–Wasserman relationship[13] described in Fig. 1(c). This interface presents a high misfit of 23% along the ⟨112⟩Au//⟨110⟩Fe direction, while in the ⟨110⟩Au//⟨001⟩Fe direction, it is only 0.6%.

The shell facets are {001}Au and {111}Au (green and red lines in Fig. 1, respectively), which are the most stable facets in fcc crystals as Au.[15,16]

These two morphologies are highly reproducible and several NPs of various nanometric sizes similar to the ones displayed in Figs. 1(a) and 1(b) can be found in Ref. 7 (and its supplemental material) and in Ref. 9. The two morphologies are not size distributed, but NPs with well-formed pyramids as in Fig. 1(a) are associated with a much larger Au amount compared to the Fe amount than the NPs with an octagonal section as in Fig. 1(b). The Au/Fe volume ratios are for instance estimated around 1.6 and 0.65, respectively, for the NPs displayed in Figs. 1(a) and 1(b).

Core–shell NPs with the same crystallographic structure and combining an almost cube-shaped core topped by pyramids as in Fig. 1(a) were also reported in the literature. Thanks to *in situ* heating, spherical Fe–Au NPs grown at room temperature transformed into an almost cube-shaped core topped by Au pyramids that are more truncated than in our experiments.[10] A core with a shape close to a FeCo cube topped by thin Au pyramids was also observed in large FeCo–Au NPs.[11] Note also that while the elastic strain relaxation can be at the origin of a strong asymmetry of the core position in the shell,[5] this mechanism seems inoperant here due to the small misfit.[9]

The deposition of pure Fe in our experimental setup leads to roughly rounded single crystals.[7] This shape is the Wulff equilibrium shape (ES) of bcc iron:[17,18] {110} and {100} facets are dominant and the ratio of their surface energy densities is close to 1, but they are truncated by differently oriented small facets, leading to an iron nanocrystal appearing rounded rather than faceted. We cannot access the detailed scenario of the NPs formation, but we can suppose that the Au shells grow on these nanocrystals.

To elucidate the Fe–Au NP morphology evolution, we investigate the energy landscape of the NPs as a function of their shape and of the Au/Fe volume ratio. For this purpose, in Sec. II, we develop a model based on the observed morphologies and we present density functional theory (DFT) calculations performed to access the energy densities of all surfaces and interfaces involved in the model. In particular, the energy of the complex {111}Au/{110}Fe interface, which is not available in the literature to our knowledge, is computed. The wetting in the Au/Fe system is predicted in Sec. III in a theoretical frame, and we compare the predicted growth mode of Au on a 2D infinite Fe substrate and on a 3D

finite Fe nanosubstrate. In Sec. IV, the equilibrium shape (ES) at constant NP volume is explored for a large Au/Fe volume ratio and a small one, and the driving forces leading to the ES, or in some cases to a metastable shape, are discussed. For this purpose, we analyze the pathways allowed in our geometrical model by the core and shell shape transformations. In Sec. V, the ES evolution with Au/Fe volume ratio is discussed and compared to experimental observations.

II. MODEL

A geometrical model describing the NP morphologies with only four independent parameters is proposed. As exploring the energy landscape of a NP requires the consideration of the energies of all surfaces and interfaces, their areas are calculated and DFT calculations of their energy densities are presented.

Note that the elastic energy due to the misfit and the grain boundary energy are not included (this will be justified later on in Sec. V E) and that the NPs are considered free of any external stress. (In our experimental setup, the NPs are formed at the surface of an amorphous Al_2O_3 substrate with which they interact, leading to the Volmer–Weber growth mode of the NPs on the substrate.[7] As for Au on alumina,[19] the adhesion of Fe–Au NPs on alumina is weak. It thus can be neglected in the determination of the NP equilibrium shape.)

A. Geometrical model of Fe–Au NPs

The geometrical model [displayed in 3D in Fig. 2(a) and in the cross section in Fig. 2(b)] is designed to allow progressive transitions between the different observed shapes.

As only {110}Fe and {001}Fe faces are involved at interfaces, we modeled the core by a polyhedron limited by 12 hexagonal {110} and 6 square {001} faces (truncated rhombic dodecahedron, in blue in Fig. 2). The respective extension of {110}Fe and {001}Fe faces can be modulated, according to the cubic symmetry. The Fe core can thus be fully described by two parameters: the Fe volume V_{Fe} and the aspect ratio

$$R_{Fe} = h^{Fe}_{110}/h^{Fe}_{001}, \quad (1)$$

where h^{Fe}_{110} and h^{Fe}_{001} are the distances from the core center to the {110}Fe and {001}Fe faces, respectively [Fig. 2(b)].

The Au shell is geometrically decomposed in a part homothetic to the core [limited in Fig. 2(b) by the interfaces on one side and by the blue dashed–dotted line on the other side] and six square based pyramids. The Au shell consists in 18 crystallites distributed on the core according to the cubic symmetry: (i) 12 are ⟨111⟩Au oriented platelets grown on the {110}Fe faces with thickness h^{Au}_{111} [in red in Fig. 2(b)]; (ii) 6 crystallites grown on the {001}Fe faces are ⟨001⟩Au oriented [in yellow in Fig. 2(b)]; each of them consists in a platelet of thickness h^{Au}_{001} topped by one square based pyramid with four {111} Au facets. The pyramid height is denoted as h^{Au}_{pyr}.

The whole shell can be fully described by two parameters, the Au volume V_{Au} and one aspect ratio to express its distribution between the homothetic shell and the pyramids. For convenience, we chose the aspect ratio f that expresses the expansion from the Fe core (in blue) to the homothetic part of the shell (blue dashed–dotted

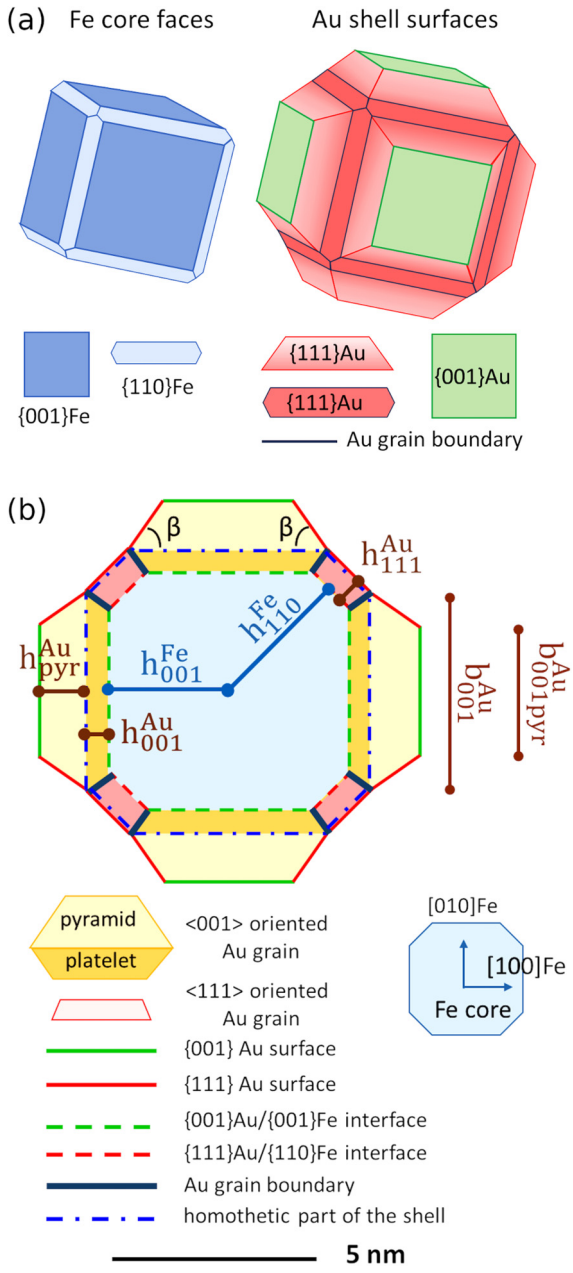

FIG. 2. Generic model of a Fe–Au NP. (a) 3D view of the Fe core and Au shell surfaces. (b) Cross section. The Fe core shape (in blue) is defined by $R_{Fe} = h^{Fe}_{110}/h^{Fe}_{001}$ [Eq. (1)]. The shell is decomposed into a part homothetic to the Fe core (limited by the blue dashed–dotted line) and six pyramids. The shell aspect ratio is defined by $f = 1 + (h^{Au}_{111}/h^{Fe}_{110}) = 1 + (h^{Au}_{001}/h^{Fe}_{001})$. The platelets filled in red on the {110}Fe faces are Au⟨111⟩ oriented crystals. The Au ⟨001⟩ oriented crystals are formed by the platelets on the {001}Fe surfaces (dark yellow) topped by square based pyramids (light yellow). The NP is built at the scale for $R_{Fe} = 1.2$, $V_{Fe} = 176$ nm^3, $f = 1.16$, $V_{Au}/V_{Fe} = 1.40$. The corresponding sizes are $h^{Fe}_{001} = 2.92$ nm, $h^{Fe}_{110} = 3.50$ nm, $h^{Au}_{001} = 0.58$ nm, $h^{Au}_{111} = 0.70$ nm and $h^{Au}_{pyr} = 1.19$ nm (or $t = 0.66$).

line). f is defined by

$$f = 1 + (h_{111}^{Au}/h_{110}^{Fe}) = 1 + (h_{001}^{Au}/h_{001}^{Fe}). \quad (2)$$

The Fe–Au NP can thus be fully described with only four independent parameters: V_{Fe} and three dimensionless parameters V_{Au}/V_{Fe}, R_{Fe}, and f.

B. Useful geometrical quantities

Let us now display geometrical quantities derived from these four parameters. These quantities will be useful to describe a NP and to calculate all surface and interface energies involved in the NP energy.

1. Core (face areas, volume)

The areas of one {001}Fe and one {110}Fe core faces (see Appendix A) are, respectively,

$$S_{001}^{Fe} = 4\,(h_{001}^{Fe})^2\left(\sqrt{2}\,R_{Fe} - 1\right)^2 \text{ and} \quad (3)$$

$$S_{110}^{Fe} = 4\,(h_{001}^{Fe})^2\left(\sqrt{2} - R_{Fe}\right)\left[\left(3\sqrt{2}/4\right)R_{Fe} - 1/2\right]. \quad (4)$$

The Fe volume is found by decomposition of the core in 18 pyramids converging at its center,

$$V_{Fe} = (6\,h_{001}^{Fe}\,S_{001}^{Fe} + 12\,h_{110}^{Fe}\,S_{110}^{Fe})/3. \quad (5)$$

It becomes

$$h_{001}^{Fe} = V_{Fe}^{1/3}\left(8 - 12\sqrt{2}\,R_{Fe}\left(\sqrt{2} - R_{Fe}\right)^2\right)^{-1/3}. \quad (6)$$

Equation (6) allows us to calculate S_{001}^{Fe} and S_{110}^{Fe} as a function of V_{Fe} and R_{Fe}.

2. Part of the Au shell homothetic to the core (areas and volume)

The areas of the top facet of a ⟨001⟩Au and of a ⟨111⟩Au oriented platelet are, respectively,

$$S_{001}^{Au} = f^2\,S_{001}^{Fe} \text{ and } S_{111}^{Au} = f^2\,S_{110}^{Fe}. \quad (7)$$

The volume of the homothetic part of the shell is

$$V_{Au}^{homo} = V_{Fe}\,(f^3 - 1). \quad (8)$$

3. Au pyramids (volume, facet areas, height, and truncation rate)

To calculate the pyramid facet areas, we introduce for convenience the dimensionless truncation rate t defined by

$$t = 1 - 2\,h_{pyr}^{Au}/(b_{001}^{Au}\,\tan\beta) = b_{001pyr}^{Au}/b_{001}^{Au}, \quad (9)$$

where $\beta = 54.7°$ is the angle between the {001}Au planes and the pyramid facets {111} $(\tan\beta = \sqrt{2})$, h_{pyr}^{Au} is the pyramid height, and b_{001}^{Au} and b_{001pyr}^{Au} are the edges of the pyramid basis and of the top facet, respectively [Fig. 2(b)]. Note that t varying from 0 (complete pyramid) to 1 (no pyramid) provides a direct description of the pyramid shape. b_{001}^{Au} is directly related to the basis area S_{001}^{Au} by

$$b_{001}^{Au} = S_{001}^{Au\,1/2} = 2\,f\,h_{001}^{Fe}\left(\sqrt{2}\,R_{Fe} - 1\right). \quad (10)$$

The volume of one pyramid V_{Au}^{pyr} can be written as a function of t as

$$V_{Au}^{pyr} = S_{001}^{Au\,3/2}\,(1 - t^3)/\left(3\sqrt{2}\right). \quad (11)$$

t can, therefore, be written as

$$t = \left[1 - 6\,V_{Au}^{pyr}/\left(\sqrt{2}\,S_{001}^{Au\,3/2}\right)\right]^{1/3}. \quad (12)$$

As V_{Au}^{pyr} is easy to write as a function of V_{Fe}, V_{Au}/V_{Fe}, and f,

$$V_{Au}^{pyr} = (V_{Au} - V_{Au}^{homo})/6 = [(V_{Au}/V_{Fe}) + 1 - f^3]\,V_{Fe}/6, \quad (13)$$

it comes from Eqs. (3), (6), and (7) that t only depends on R_{Fe}, V_{Au}/V_{Fe}, and f. The areas of one lateral {111}Au facet S_{111pyr}^{Au} and of the top {001}Au facet S_{001pyr}^{Au} are

$$S_{111pyr}^{Au} = (1 - t^2)\,S_{001}^{Au}/(4\,\cos\beta) \text{ and } S_{001pyr}^{Au} = t^2\,S_{001}^{Au}. \quad (14)$$

It is important to keep in mind that once R_{Fe}, V_{Au}/V_{Fe}, and f are fixed, there exists a unique distribution of the gold in the homothetic shell and the pyramids (there is a unique correspondence between f and t). All the geometrical quantities defined here (distances, areas, and volumes) depend on V_{Fe}, V_{Au}/V_{Fe}, R_{Fe}, and f.

C. Limits of the aspect ratios

As the core is a polyhedron limited by {001}Fe and {110}Fe faces within the cubic symmetry, R_{Fe} varies from $1/\sqrt{2}$ (perfect rhombic dodecahedron built with 12 {110}Fe lozenges) to $\sqrt{2}$ (perfect cube built with 6 {001}Fe squares) [Fig. 3(a)].

The limits of f, f_{min}, and f_{max}, depend on V_{Au}/V_{Fe} and R_{Fe} (see Appendix B). We also calculate the limits t_{min} and t_{max} of the pyramid truncation t, which is a monotonous and increasing function of f. When Au is entirely distributed in the homothetic part of the shell, f and t reach their maxima f_{max} and t_{max},

$$f_{max} = [1 + (V_{Au}/V_{Fe})]^{1/3} \quad ; \quad t_{max} = 1. \quad (15)$$

When the Au pyramids are as complete as possible, f and t reach their minima f_{min} and t_{min}. As illustrated in Fig. 3(b) for a particular R_{Fe} and three different volume ratios, these minima are

(i) $1 < f_{min} < f_{max}$ and $t_{min} = 0$ if the wetting layer still exists when the pyramids are complete,

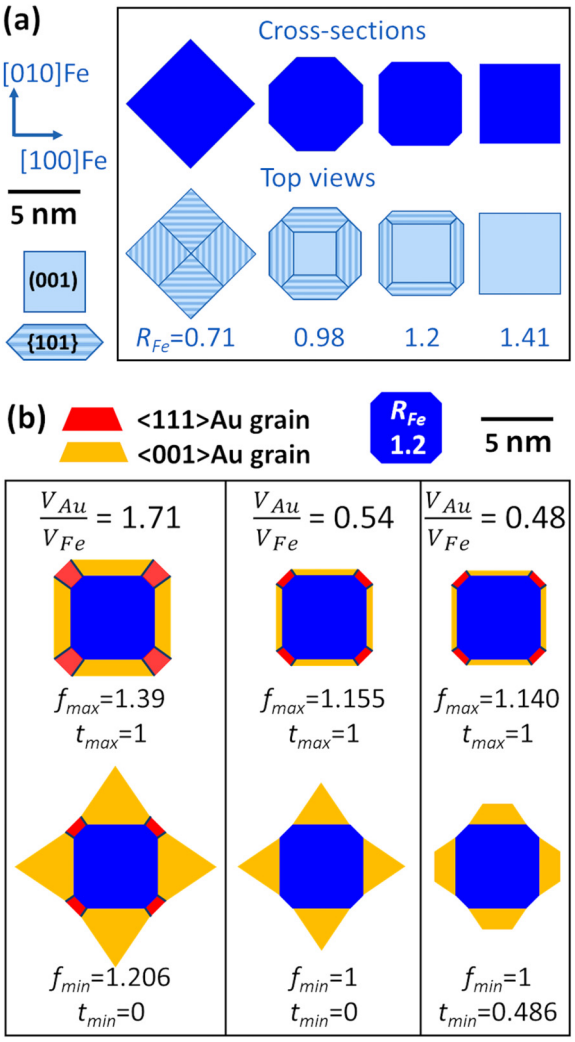

FIG. 3. (a) Cross section (top) and top-view (bottom) of the core for various aspect ratios R_{Fe} from $1/\sqrt{2}$ to $\sqrt{2}$. (b) Geometrical limits of the shell, illustrated in the cross section with $R_{Fe} = 1.2$ for various volume ratios V_{Au}/V_{Fe}. The scale is for $V_{Fe} = 175.6$ nm^3 (same order of magnitude as the average experimental volumes in Ref. 7).

(ii) $f_{min} = 1$ and $t_{min} = 0$ when the completion of the pyramids coincides with an empty wetting layer, and
(iii) $f_{min} = 1$ and $0 < t_{min} < 1$ if pyramids cannot be complete even without wetting layer.

The exact calculation of f_{min} and t_{min} is given in Appendix B.

D. Experimental analysis with the geometrical model

Average values of R_{Fe}, h^{Fe}_{001}, h^{Au}_{111}, and h^{Au}_{pyr} of a single NP can be measured from high resolution transmission electron microscopy (HRTEM) images. V_{Fe}, f, and V_{Au}/V_{Fe} are then deduced through Eqs. (2), (6), and (13). The models represented in Fig. 1 are built with the measures from the experimental images and are displayed at the same scale.

For Fig. 1(a), the measured values used to build the model are $R_{Fe} = 1.35 \pm 0.04$, $h^{Fe}_{001} = 2.2 \pm 0.1$ nm, $h^{Au}_{111} = 0.41 \pm 0.1$ nm and an average $t = 0.66$ (or $h^{Au}_{pyr} = 1.1$ nm). We thus estimate $V_{Fe} \approx 84$ nm^3, $f \approx 1.14$, and $V_{Au}/V_{Fe} \approx 1.6$ in this single NP. Estimates of V_{Au}/V_{Fe} in several other NPs from Refs. 7 and 9 (and the supplemental material of Ref. 7) with the same morphology as in Fig. 1(a) are in the range of 1.6–2.3. The {111}Au/{110}Fe interfaces barely even exist and the core corners are covered by two or more Au MLs.

For Fig. 1(b), the measured values used to build the model are $R_{Fe} = 0.98 \pm 0.02$, $h^{Fe}_{001} = 3.26 \pm 0.1$ nm, $h^{Au}_{111} = 0.58 \pm 0.1$ nm, and $h^{Au}_{pyr} \approx 0$, giving directly $t \approx 0$ and $f \approx 1$. The deduced Fe volume is 168 ± 25 nm^3 and the deduced volume ratio V_{Au}/V_{Fe} in this single NP is 0.65 ± 0.15.

These estimations indicate that the Au/Fe ratio in NPs with well-formed pyramids is three to four times larger than in NPs as in Fig. 1(b).

E. Surface and interface energy densities

To investigate the energy landscape of a NP with the geometrical model, the surface and interface energies densities, defined as excess energies compared to bulk phases, are necessary. They were calculated with the density functional theory (DFT) with the methodology described in Refs. 20 and 21 and are reported in Table I.

1. DFT calculations

Spin-polarized DFT calculations have been performed using the VASP code, with projector augmented wave method (PAW) pseudopotentials and the Perdew-Burke-Ernzerhof (PBE) functional. The cutoff energy has been set to 600 eV for all calculations and a Methfessel–Paxton smearing with σ 0.05 eV was used. A Monkhorst–Pack mesh of special k-points has been determined in order to achieve the convergence of the energy up to 2 meV/atom for each investigated system. Periodic boundary conditions are used in the x, y, and z directions, and the two slabs are separated from their images by adding 1.5 nm of vacuum in the z-direction.

TABLE I. Surface and interface energy densities obtained from DFT calculations with the PBE functional and experimental data.

	DFT–PBE	Experimental
γ^{Au}_{001}	0.873 J/m^2	
γ^{Au}_{111}	0.734 J/m^2	≈1.5 J/m^2 [15]
$\gamma^{Au}_{111}/\gamma^{Au}_{001}$	0.84	0.84[a]
γ^{Fe}_{001}	2.478 J/m^2	
γ^{Fe}_{110}	2.428 J/m^2	2.417 J/m^2 [23]
$\gamma^{Fe}_{110}/\gamma^{Fe}_{001}$	0.98	≈1 [17]
$\gamma^{interf}_{(001)Au/(001)Fe}$	0.378 J/m^2	
$\gamma_{(111)Au/(110)Fe}$	0.700 J/m^2	

[a]Found by application of the Wulff theorem to the Au nano-island of Ref. 22.

The atomic positions were relaxed until the forces reach a value lower than 10^{-2} eV Å^{-1}.

As discussed in Ref. 20, the (001)Au and (111)Au surface energies, γ_{001}^{Au} and γ_{111}^{Au}, respectively, are underestimated with respect to the experimental values (around 1.5 J/m^2).[15] This is due to the use of the PBE exchange and correlation functional that, although giving excellent results in reproducing the properties of iron, is not very performing for gold. However, the ratio $\gamma_{111}^{Au}/\gamma_{001}^{Au}$ is in excellent agreement with the experimental estimates; for instance, a 0.84 ratio is deduced applying the Wulff theorem to the Au nanoisland from Ref. 22. For (001)Fe and (110)Fe, the surface energies, γ_{001}^{Fe} and γ_{110}^{Fe}, respectively, are in very good agreement with the experiments.[18,23]

For the energy density of the {001}Au/{001}Fe interface, $\gamma^{interf}_{(001)Au/(001)Fe}$, we used the same model of coherent interface as in Refs. 20 and 21. For the energy density of the {111}Au/{110}Fe interface, $\gamma^{interf}_{(111)Au/(110)Fe}$, we developed a new model reproducing the epitaxial Nishiyama–Wasserman relationship[7,13] with periodic boundary conditions. As a first approximation, we chose to model this interface using a semi-coherent approach in the [101] direction as proposed by Lu *et al.* for the (111)Ag/(110)Fe interface.[24] The coincidence between the two lattices along the [110] direction is five Fe cells for four Au cells (5 × 4). After optimization, the system exhibits an interface dislocation enabling to accommodate a large part of the high lattice misfit in this direction. A more detailed study will be reported elsewhere. For both interfaces, the energies were converged within ±10 mJ/m^2 for a slab with 12 Fe MLs and more than 4 Au MLs.

2. Dependence with the Au thickness

The excess energy experienced by an iron surface covered by Au is due to the Au surface energy and interface energy. However, to explore the case of small Au/Fe volume ratios [Fig. 3(b)], it is mandatory to consider the possibility for Fe surfaces to be bare (the excess energy is then due to $\gamma_{surface}^{Fe}$) and to introduce a progressive transition from the bare Fe surface to the full wetting by Au. For the sake of simplicity, we chose to monitor the full wetting condition with a single parameter, a critical Au thickness. In the following, for Au thicknesses larger than this critical value, the surface and interface energies are calculated with the densities $\gamma_{surface}^{Au}$ and $\gamma_{interface}$ from Table I. Below the critical thicknesses, we impose a linear increase in $\gamma_{surface}^{Au}$ and $\gamma_{interface}$ as the Au thickness decreases until $\gamma_{surface}^{Au} + \gamma_{interface}$ becomes equal to $\gamma_{surface}^{Fe}$ when the Au thickness is null, as described in Fig. 4. We fixed the critical thicknesses at two MLs (0.46 nm for {111}Au and 0.40 nm for {001}Au) corresponding to the minimal Au coverage experimentally observed in our NPs.

III. GROWTH MODES OF GOLD ON INFINITE 2D AND FINITE 3D IRON SUBSTRATES

The growth mode of the Au/Fe system can be predicted on the basis of our DFT calculated surface and interface energies. Beyond the classical case of the growth on a 2D infinite substrate, our aim in this section is to discuss the growth mode when the substrate is a 3D nanocrystal of finite size.

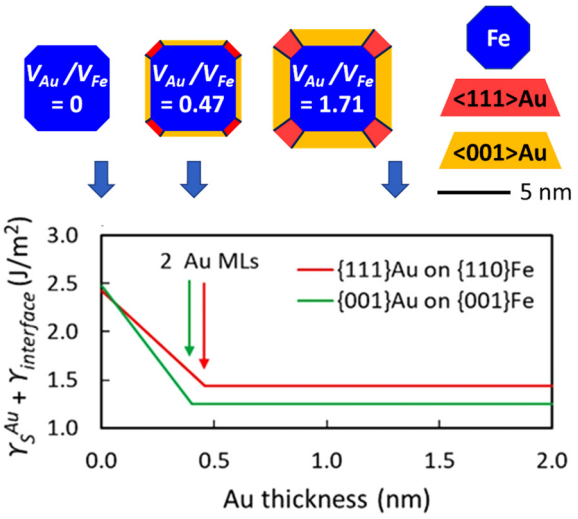

FIG. 4. $\gamma_{surface}^{Au} + \gamma_{interface}$ as a function of the gold thickness. If the Au layer exceeds a critical thickness, chosen here to be two MLs, $\gamma_{surface}^{Au}$ and $\gamma_{interface}$ are the DFT computed data (Table I). Below the critical thickness, a linear increase is imposed to $\gamma_{surface}^{Au}$ and $\gamma_{interface}$ so that for the bare iron, $\gamma_{surface}^{Au} + \gamma_{interface}$ is equal to $\gamma_{surface}^{Fe}$ (DFT data from Table I). The illustrations are NPs with $R_{Fe} = 1.2$. For $V_{Fe} = 175.6$ nm^3 the Au/Fe volume ratios correspond from left to right to bare iron, Au thickness around the critical thickness, and larger Au thickness, here around 1.3 nm (six MLs).

A. Growth mode of Au on an infinite 2D Fe substrate

The wetting factor $\Phi_{Au/Fe}$ that expresses the balance of surface and interface energies involved in the formation of a 2D Au layer on a 2D Fe substrate is[13]

$$\Phi_{Au/Fe} = \gamma_{surface}^{Au} + \gamma_{interface} - \gamma_{surface}^{Fe}. \quad (16)$$

The growth mode (in near-equilibrium conditions) is predicted from the sign of $\Phi_{Au/Fe}$: 2D Frank van der Merwe (full wetting) if negative or 3D Volmer–Weber (partial wetting) if positive. It is also interesting to calculate the adhesion energy of the Au/Fe system,

$$W_{ad} = \gamma_{surface}^{Au} - \gamma_{interface} + \gamma_{surface}^{Fe}. \quad (17)$$

Thanks to the DFT calculated energies of both {111}Au/{110}Fe and {001}Au/{001}Fe interfaces, we are able to predict and compare quantitatively their growth modes. Table II reports the adhesion energies and the wetting factors of Au on Fe calculated with the surface and energies DFT computed data of Table I.

Both interfaces have a high adhesion energy. The largest adhesion energy of {001}Au/{001}Fe compared to {111}Au/{110}Fe is due for one-third to the difference in γ_{111}^{Au} and γ_{001}^{Au} and for two-thirds to the difference in $\gamma^{interf}_{(111)Au/(110)Fe}$ and $\gamma^{interf}_{(111)Au/(110)Fe}$. The negative wetting factors in Table II induced that for the two considered Fe orientations, the growth mode of Au on Fe system predicted by DFT is 2D Frank van der Merwe, i.e., the 2D Au layer is formed even for null sursaturation. In addition, the absolute values of the wetting factors are comparable to the corresponding Au surface energies, which indicate a strong tendency to Au on Fe wetting.

TABLE II. Adhesion energies W_{ad} of the Au/Fe interfaces and wetting factors $\Phi_{Au/Fe}$ of Au on Fe, and $\Phi_{Fe/Au}$ of Fe on Au, calculated from the DFT computed data of Table I.

Interface		DFT–PBE (J/m^2)
(111)Au/(110)Fe	W_{ad}	2.462
(001)Au/(001)Fe	W_{ad}	2.973
(111)Au on (110)Fe	$\Phi_{(111)Au/(110)Fe}$	−0.994
(001)Au on (001)Fe	$\Phi_{(001)Au/(001)Fe}$	−1.227
(110)Fe on (111)Au	$\Phi_{(110)Fe/(111)Au}$	2.394
(001)Fe on (001)Au	$\Phi_{(001)Fe/(001)Au}$	1.983

Table II also reports the wetting factors of iron on gold. They are much larger than for gold on iron, positive values even suggesting a Volmer–Weber growth mode of iron on gold (i.e., partial wetting). Combined to the low miscibility of the two metals, here this fully preserves the initial iron NPs as cores for the further growth of gold shell. More generally, this clearly favors a Fe(core)-Au(shell) chemical order in this system.

B. Growth of Au on a finite 3D Fe nano-substrate: From a 2D growth mode to a 3D Stranski–Krastanov (SK)-like growth mode

Within our geometrical model, we can calculate precisely the variation of free energy ΔF needed to form an Au shell on a Fe nano-substrate of predefined shape and finite size. To condensate n atoms from Au vapor as a shell with a homogeneous thickness, ΔF is

$$\Delta F = E^{Au}_{surface} + E_{interface} - E^{Fe}_{surface} - n\Delta\mu, \tag{18}$$

where $E^{Au}_{surface}$ and $E_{interface}$ are the costs in Au surfaces and Au/Fe interfaces to form an Au shell, $(-E^{Fe}_{surface})$ is the gain provided by the full wetting of Fe by Au, and $\Delta\mu$ is the difference of chemical potential of gold between the vapor and the solid phase. To ensure the constraint on the homogeneous shell thickness, we consider here that the shell adopts the same shape as the core so that f is fixed to f_{max} [defined by Eq. (15) in Sec. II C]. It becomes

$$E^{Fe}_{surface} = 12\,\gamma^{Fe}_{110}\,S^{Fe}_{110} + 6\,\gamma^{Fe}_{001}\,S^{Fe}_{001}, \tag{19}$$

$$E^{Au}_{surface} = 12\,\gamma^{Au}_{111}\,S^{Au}_{111} + 6\,\gamma^{Au}_{001}\,S^{Au}_{001}, \tag{20}$$

$$E_{interface} = 12\,\gamma^{interf}_{(111)Au/(110)Fe}\,S^{Fe}_{110} + 6\,\gamma^{interf}_{(001)Au/(001)Fe}\,S^{Fe}_{001}, \tag{21}$$

$$\Delta F = 12\,(\gamma^{interf}_{(111)Au/(110)Fe} + f^2_{max}\,\gamma^{Au}_{111} - \gamma^{Fe}_{110})S^{Fe}_{110} + 6\,(\gamma^{interface}_{(001)Au/(001)Fe} + f^2_{max}\,\gamma^{Au}_{001} - \gamma^{Fe}_{001})S^{Fe}_{001} - n\Delta\mu. \tag{22}$$

It is interesting to define $\Phi_{Au/(3D)Fe}$ by dividing the surface and interface contributions by the core area,

$$\Phi_{Au/(3D)Fe} = \frac{E^{Au}_{surface} + E_{interface} - E^{Fe}_{surface}}{12\,S^{Fe}_{110} + 6\,S^{Fe}_{001}} = \frac{(\gamma^{interf}_{(111)Au/(110)Fe} + f^2_{max}\,\gamma^{Au}_{111} - \gamma^{Fe}_{110})(\sqrt{2} - R_{Fe})(3\sqrt{2}R_{Fe} - 2) + 2(\gamma^{interf}_{(001)Au/(001)Fe} + f^2_{max}\,\gamma^{Au}_{001} - \gamma^{Fe}_{001})(\sqrt{2}R_{Fe} - 1)^2}{(\sqrt{2} - R_{Fe})(3\sqrt{2}R_{Fe} - 2) + 2(\sqrt{2}R_{Fe} - 1)^2}. \tag{23}$$

Note that $\Phi_{Au/(3D)Fe}$ is nothing else than the wetting factor adapted to the 3D morphology of the nanosubstrate. In contrast with a 2D infinite substrate, here the wetting factor depends on the Au deposited volume. Indeed, f_{max} is related to V_{Au}/V_{Fe} through Eq. (15). $\Phi_{Au/(3D)Fe}$ is displayed in Fig. 5 as a function of V_{Au}/V_{Fe} for various R_{Fe} from $1/\sqrt{2}$ to $\sqrt{2}$. For a small volume ratio, it comes from Eq. (15) that f_{max} tends to 1, so that $\Phi_{Au/(3D)Fe}$ reduces to the average value of $\Phi_{Au/Fe}$ weighted by the respective surface areas of the two types of crystallites and is negative whatever the Fe nanocrystal shape.[29] The wetting factor $\Phi_{Au/(3D)Fe}$ then increases linearly with f^2_{max} with a R_{Fe} dependency.[30] There exists a critical value $f_{critical}$ and a critical volume ratio for which $\Phi_{Au/(3D)Fe}$ becomes null,

$$f_{critical} = \left[-\frac{(\gamma^{interf}_{(111)Au/(110)Fe} - \gamma^{Fe}_{110})(\sqrt{2} - R_{Fe})(3\sqrt{2}R_{Fe} - 2) + 2(\gamma^{interf}_{(001)Au/(001)Fe} - \gamma^{Fe}_{100})(\sqrt{2}R_{Fe} - 1)^2}{\gamma^{Au}_{111}(\sqrt{2} - R_{Fe})(3\sqrt{2}R_{Fe} - 2) + 2\,\gamma^{Au}_{100}(\sqrt{2}R_{Fe} - 1)^2}\right]^{1/2}, \tag{24}$$

$$(V_{Au}/V_{Fe})_{critical} = (f_{critical})^3 - 1. \tag{25}$$

The critical volume ratio is between 2.6 and 2.7 depending on R_{Fe} (Fig. 5). Below the critical ratio, the shell formation with a full wetting provides a gain in energy as in the classical 2D Frank–van der Merwe growth mode. This also means that, once formed, a Fe(core)–Au(shell) NP should be very stable against partial dewetting. [Note that the $\gamma^{Au}_{surface}$ being underestimated compared to

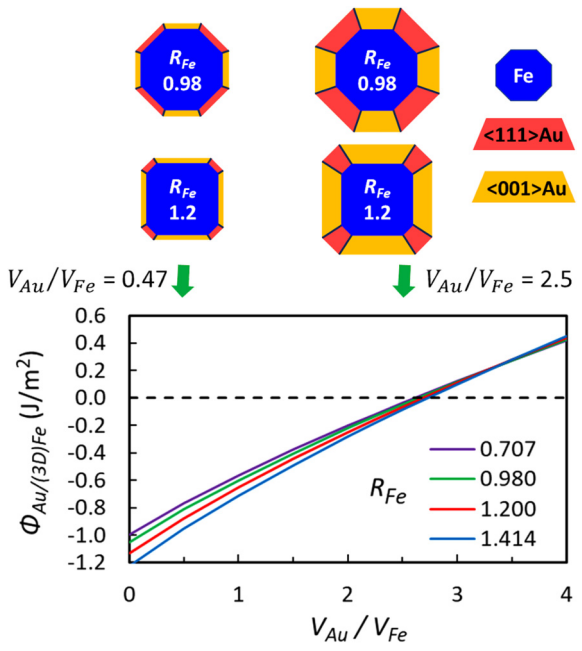

FIG. 5. Wetting factor $\Phi_{Au/(3D)Fe}$ adapted to the 3D morphology of the nanosubstrate, calculated as a function of the Au/Fe volume ratio for various Fe core shapes. The energies densities used are those calculated by DFT–PBE (Table I). The illustrations are for $R_{Fe} = 0.98$ and 1.2 and the two volume ratios 0.47 and 2.5.

experimental data (Table I), the wetting factor predicted could also be underestimated. However, the full wetting is experimentally attested in the NPs from Ref. 25 and from our work.]

Above, $\Phi_{Au/(3D)Fe}$ is positive and the growth requires an increasing positive sursaturation.

Here we can make an analogy with the 3D Stranski–Krastanov (SK) growth mode, the third classical growth mode adopted by a film grown on an infinite 2D substrate (in near-equilibrium conditions).[13] In the SK growth mode, the wetting is complete and the layer first grows 2D; then after a so-called critical thickness, islands take place on the wetting layer. It has been formally described by considering that the wetting factor, negative at first at the onset of the growth, increases with the deposited thickness so that it becomes positive.[13,26] In strained semiconducting heterostructures, where the SK growth mode is often observed, this increase is due to the integration in the wetting factor of the elastic energy, a term proportional to the deposited thickness.[13,26] The driving force for a 3D morphology is thus the relaxation of the elastic energy by the island faces.[26,27]

In our model, the increase of the wetting factor $\Phi_{Au/(3D)Fe}$ with the Au/Fe volume ratio and the change of its sign is due to the shell surface increase. Note that this phenomenon is expected independently of the core and shell crystallography. However, a 3D SK-like growth mode will occur only if a modulation of the shell thickness decreases this wetting factor. As investigated in Sec. IV, this will be possible here thanks to the polycrystalline character of the shell engendered by the accommodation of its crystallographic lattice (fcc) to the core one (bcc).

IV. EQUILIBRIUM SHAPE OF THE FE–AU NANOPARTICLES AT CONSTANT VOLUMES

In this section, we determine the equilibrium shape (ES) of a NP of given Au and Fe volumes, and we identify the driving forces at the origin of the shape transformations allowed in our geometrical model. For this purpose, we analyze the pathways leading to the ES. We consider as initial configurations the cases where the shell adopts the same external shape as the core, i.e., when $f = f_{max}$ as in Sec. III. Then, we assume that a shape transformation can only occur by progressive change of R_{Fe} and/or f.

A large Au/Fe volume ratio of 1.71 is first considered then a small one of 0.57.

A. Excess energy of a nanoparticle

The excess energy of the NP compared to the same Au and Fe volumes in their bulk phases is

$$E_{NP} = E^{Au}_{surface} + E_{interface} \tag{26}$$

While $E_{interface}$ is the same as in Sec. III B, here the surface contribution includes the pyramid facets,

$$E^{Au}_{surface} = 12\ \gamma^{Au}_{111}\ S^{Au}_{111} + 6\ (\gamma^{Au}_{001} S^{Au}_{001pyr} + 4\ \gamma^{Au}_{111}\ S^{Au}_{111pyr}), \tag{27}$$

$$E_{interface} = 12\ \gamma^{interf}_{(111)Au/(110)Fe}\ S^{Fe}_{110} + 6\ \gamma^{interf}_{(001)Au/(001)Fe}\ S^{Fe}_{001}. \tag{28}$$

The solutions of the energy minimization as a function of the two aspect ratios R_{Fe} and f are numerically determined for a Fe volume $V_{Fe} = 175.6\ nm^3$. The core edge when the shape is a cube is 5.6 nm that corresponds to the average experimental value.[7] The core aspect ratio R_{Fe} varies from $1/\sqrt{2}$ (perfect rhombic dodecahedron with 12 {110}Fe faces) to $\sqrt{2}$ (perfect {001}Fe oriented cube). As discussed in Sec. II C, the upper limit of f is f_{max} from Eq. (15) (the whole Au volume is distributed in the homothetic shell); then, f can be lowered by the progressive building of the pyramids up to f_{min}.

B. Equilibrium shape for a large Au/Fe volume ratio

We present in detail the case of $V_{Au}/V_{Fe} = 1.71$ with $V_{Fe} = 175.6\ nm^3$. Figure 6 displays the total excess energy E_{NP} as a function of the two aspect ratios R_{Fe} and f. The upper limit of f, common to all R_{Fe} values, is $f_{max} = 1.39$ [from Eq. (15)]. For all R_{Fe}, the Au/Fe volume ratio is large enough to build untruncated pyramids ($t = 0$) without completely emptying the homothetic shell (f remains strictly larger than 1).

As long as R_{Fe} is lower than 1, the minimum of energy is for f_{max} (shape without pyramids). For a given core shape R_{Fe} larger than 1, the minimum is for a lower f, demonstrating the possibility of a 3D SK-like growth mode, where a part of the shell is transferred into pyramids at the detriment of the homothetic shell.

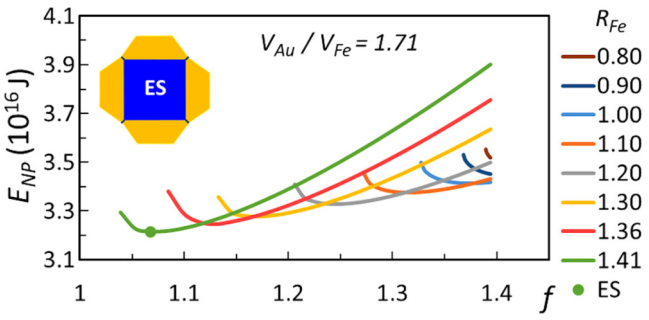

FIG. 6. Excess energy of a single NP with $V_{Fe} = 175.6$ nm^3 and $V_{Au}/V_{Fe} = 1.71$, displayed as a function of f and R_{Fe}. $f_{max} = 1.39$ corresponds to a homothetic shell without pyramids. The ES ($R_{Fe} = \sqrt{2}$ and $f = 1.073$ or $t = 0.535$) is shown.

Comparing the different core shapes, it is then seen that the minimum of E_{NP} is for $R_{Fe} = \sqrt{2}$ (cube-shaped core) and $f = 1.073$. The homothetic shell thickness under the pyramids h^{Au}_{001} and the pyramid height h^{Au}_{pyr} are then, respectively, 0.21 nm (about 1 {001} Au ML) and 1.98 nm (about 10 {001}Au MLs) and the truncation $t = 0.535$. This ES is displayed in the inset.

C. From initial shapes to optimal shapes for a large Au/Fe volume ratio

To analyze the driving forces leading to this ES, we report in Fig. 7 (blue curve) the excess energies of NPs with a homogeneous shell thickness ($f = f_{max}$ or $t = 1$). The four core shapes illustrated in Fig. 7 are $R_{Fe} = 1/\sqrt{2}$, 1.015, 1.2, and $\sqrt{2}$. The possible pathways reducing E_{NP} at constant volumes from these initial configurations are then decomposed in two distinct shape transformations. The excess energies are taken from Fig. 6.

(i) 2D–3D Stranski–Krastanov-like transition: This transformation consists in building ⟨001⟩Au oriented pyramids at the detriment of ⟨111⟩Au oriented platelets, the core shape being unchanged (golden arrows). The driving force to form pyramids is the reduction of surface energy by increasing the part of {111}Au surfaces compared to {001}Au (respectively the lateral and top facets of the pyramids). We call this mechanism a 2D–3D SK-like transition because it reduces the effective wetting factor by the modulation of the shell thickness. This mechanism is active only for R_{Fe} larger than 1.

(ii) Core shape transformation: One possible driving force is the reduction of the interface energy. The core shape minimizing the interface energy $E_{interface}$ is found by application of the Wulff theorem and is $R_{Fe} = \gamma^{interf}_{(111)Au/(110)Fe}/\gamma^{interf}_{(001)Au/(001)Fe}$. As this ratio is larger than $\sqrt{2}$ here (from Table I), the {111} Au/{110}Fe interfaces are unstable against {001}Au/{001}Fe interfaces and should disappear at the benefit of the shape of a cube. However, this would be true only without surface effects. Indeed the cost due to larger {001}Au facets with the shape of a cube could be uncompensated by the gain in interface energy. As a consequence, it is seen in Fig. 7 that as long as the shell thickness is homogeneous ($t = 1$ or $f = f_{max}$), the minimum of energy for R_{Fe} is around 1. Actually, this optimal core shape can be found analytically with the Wulff theorem, by considering that each core face experiences the interface energy plus the surface energy of the Au platelet above, and is

$$R^{homo}_{Fe} = \frac{\gamma^{interf}_{(111)Au/(110)Fe} + f^2_{max}\,\gamma^{Au}_{111}}{\gamma^{interf}_{(001)Au/(001)Fe} + f^2_{max}\,\gamma^{Au}_{001}}. \quad (29)$$

Here, with $V_{Au}/V_{Fe} = 1.71$ it comes $R^{homo}_{Fe} = 1.025$. The blue arrows in Fig. 7 indicate the pathway from various initial core shapes toward this minimum, the shell thickness remaining homogeneous.

(iii) Finally, the two mechanisms of transformation can cooperate and the minimum of energy can be reached by simultaneous changes in R_{Fe} and f as illustrated by the green arrows. The ES combines the cube-shaped core minimizing the interface energy and the {001}Au pyramids optimizing the ratio between the areas of the two gold facet types.

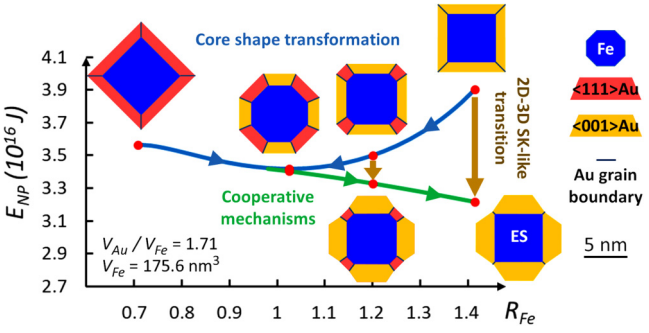

FIG. 7. Shape transformations reducing the NP energy at constant Au and Fe volumes, for large volume ratios. The illustrations are at the scale for $V_{Fe} = 175.6$ nm^3 and $V_{Au}/V_{Fe} = 1.71$.

In our model, the bare iron is characterized applying the Wulff theorem by an aspect ratio $R^{Wulff}_{Fe} = \gamma^{Fe}_{110}/\gamma^{Fe}_{001}$. If, at the onset of the shape transformation, the core is close to this value (0.98 from Table I), it can easily evolve toward R^{homo}_{Fe} (1.025), these two values being by chance very close. As the pyramid formation also begins around $R_{Fe} = 1$, the two mechanisms cooperate leading to the ES.

D. Equilibrium shape for a small Au/Fe volume ratio

Figure 8 displays the NP excess energy for the small ratio $V_{Au}/V_{Fe} = 0.57$. Here, $f_{max} = 1.162$. As for larger volume, for a given core shape R_{Fe} larger than about 1, the minimum is not obtained for the homogenous shell thickness. Allowing change in R_{Fe}, there exist two minima (the corresponding shapes are shown in the inset). The first minimum (M1) presents the same shape (cube) for the iron core as for the large volume ratio. The

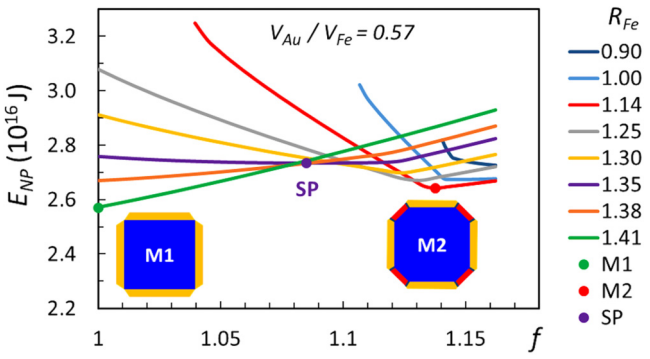

FIG. 8. Excess energy of a single NP with $V_{Fe} = 175.6$ nm^3 and $V_{Au}/V_{Fe} = 0.57$ displayed as a function of f and R_{Fe}. $f_{max} = 1.162$ corresponds to a homothetic shell without pyramids. The shapes in inset correspond to the M1 minimum ($R_{Fe} = \sqrt{2}$ and $f = 1$) and M2 minimum ($R_{Fe} = 1.14$ and $f = 1.135$). SP is the saddle point ($R_{Fe} = 1.35$).

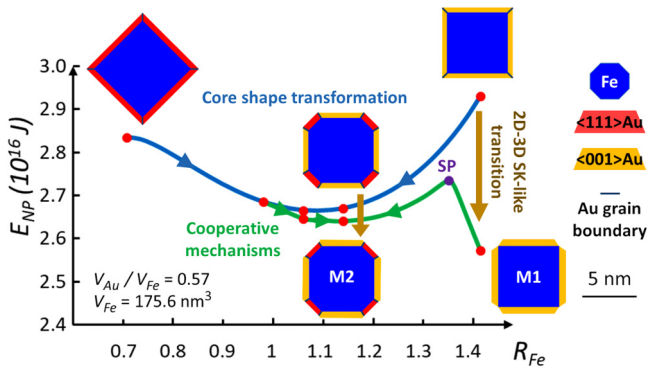

FIG. 9. Shape transformations reducing the NP energy at constant Au and Fe volumes, for small volume ratios. The illustrations are at the scale for $V_{Fe} = 175.6$ nm^3 and $V_{Au}/V_{Fe} = 0.57$.

homothetic shell, however, is empty ($f = 1$) and Au is entirely distributed in 0.62 nm thick pyramids (about three {001}Au MLs). The truncation is $t = 0.842$.

The second minimum (M2) is for $R_{Fe} = 1.14$ and $f = 1.135$. The homothetic shell thicknesses are $h_{111}^{Au} = 0.46$ nm and $h_{001}^{Au} = 0.4$ nm, i.e., two MLs. The ⟨001⟩ oriented Au platelets are covered by flat pyramids with height $h_{pyr}^{Au} = 0.2$ nm (about one {001}Au MLs) and truncation $t = 0.934$. The existence of this second minimum is related to the increase introduced in surface and interface energies for low h_{111}^{Au} to account for the transition between full wetting and bare iron as described in Sec. II E 2 (Fig. 4). Indeed, while the NPs examined in Secs. IV B and IV C always experience the full wetting for any explored shape (Au thickness always larger than two MLs), here the reduction of V_{Au}/V_{Fe} dramatically reduces the ability to form a full Au wetting layer for any explored shape. In other words, the Au layer is thinner than two MLs for some sets of aspect ratios (f, R_{Fe}).

E. From initial shapes to optimal shapes for a small Au/Fe volume ratio

Figure 9 describes the possible pathway to ES from initial shapes with homogeneous shells (E_{NP} are taken from Fig. 8). The blue curve displays E_{NP} when the shell thickness is homogeneous ($f = f_{max}$). Its minimum is given by Eq. (29) and is $R_{Fe}^{homo} = 1.086$ for $V_{Au}/V_{Fe} = 0.57$. As a reduction of E_{NP} by pyramid formation is possible from about $R_{Fe} = 1$, the minimum M2 is achieved by the cooperation of core transformation and pyramid development (green arrow). M1 and M2, however, are separated by a saddle point (SP) of the first order located at $R_{Fe} = 1.35, f = 1.09$ (from Fig. 8). The barrier between M2 and SP is so high (9×10^{-18} J or 58 eV) that it fully prevents the transition from M2 to M1 through the geometrical transformations included in our model. The minimum M1 could be achieved from the initial shape of a cube by the pyramid formation (golden arrow).

V. DISCUSSION AND COMPARISON WITH EXPERIMENTAL NANOPARTICLES

We then explore the ES as a function of the Au/Fe volume ratio from 0.47 to 2.5. Figure 10 displays the evolution of R_{Fe} (a), t (b), and Au thicknesses (c) for the two minima M1 and M2 as a function of the volume ratio. Here, we chose to represent the shell shape through t rather than f, because t provides a direct focus on the pyramid shape. To predict the shape evolution, we describe and discuss separately the evolution of the M1 and M2 minima and then we discuss which minimum is likely to form at each volume ratio.

A. Evolution of the optimal shape M1 toward an optimal truncation

The M1 minimum (green curves in Fig. 10) exists for all volume ratios. While the core shape is consistently a cube, there exist two regimes for the shell shape.

(i) For volume ratio below 1.2: The homothetic layer below the pyramids is empty [$h_{001}^{Au} = 0$ in Fig. 10(c), corresponding to $f = 1$]. The Au volume increase entirely contributes to develop the ⟨001⟩ oriented pyramids as shown by the progressive decrease of the truncation [Fig. 10(b)] and the corresponding increase of h_{pyr}^{Au} [Fig. 10(c)].

(ii) For volume ratio above 1.2: When V_{Au}/V_{Fe} reaches 1.2, the truncation reaches 0.534. Then, the shell morphology changes with the apparition of the homothetic layer. As seen in Fig. 10(c) (green curves), the increase in the volume ratio above 1.2 indeed results in the concomitant thickens of the layers under the pyramids (h_{001}^{Au}) and increase of the pyramid height (h_{pyr}^{Au}). It is important to note that the truncation does no more evolve [Fig. 10(b)], meaning that the pyramid shape (above the homothetic shell) is unchanged.

These different steps are illustrated at the same scale in Fig. 11 (green squares) on which one can see that the homothetic layer is absent and all the gold is within the truncated pyramids up to $V_{Au}/V_{Fe} = 1.2$.

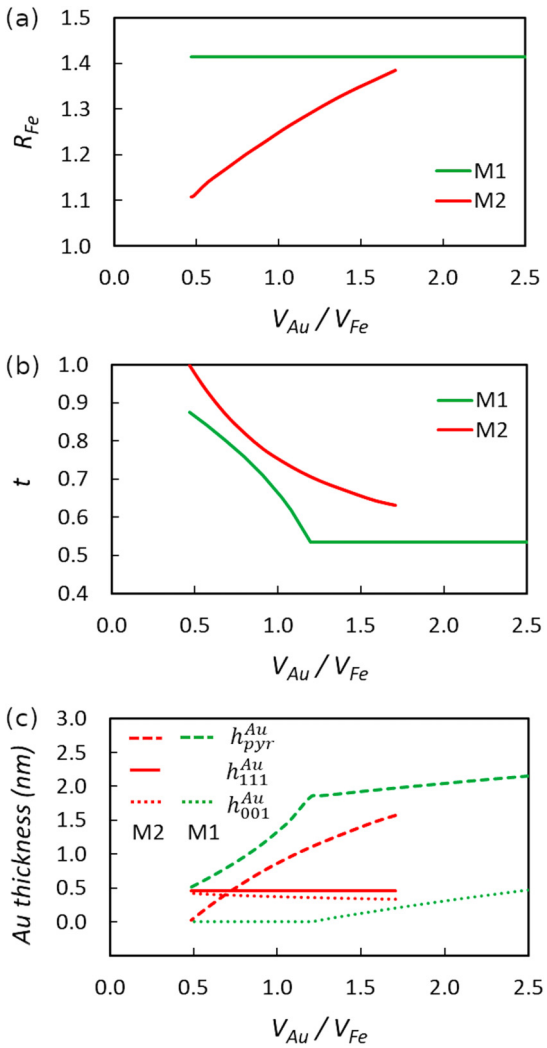

FIG. 10. Evolution of R_{Fe} (a), t (b), and Au thicknesses (c) for the two minima M1 and M2 as a function of the Au/Fe volume ratio (for $V_{Fe} = 175.6$ nm^3).

Beyond 1.2, we observe the appearance of the homothetic layer and the stabilization of the truncation at $t_{opt} = 0.534$.

B. Evolution of the optimal shape M2

For $V_{Fe} = 175.6$ nm^3, the M2 minimum (red curves in Fig. 10) exists from $V_{Au}/V_{Fe} = 0.47$, which is the minimal ratio ensuring a full wetting with two MLs: the pyramids are indeed empty ($h^{Au}_{pyr} = 0$ and $t = 1$). Then, the core shape evolves monotonically from $R_{Fe} = 1.11$ for $V_{Au}/V_{Fe} = 0.47$ to $R_{Fe} = 1.39$ for $V_{Au}/V_{Fe} = 1.7$ [Fig. 10(a)]. At the same time, the thickness of the ⟨111⟩ oriented Au platelets [h^{Au}_{111} in Fig. 10(c)] is stable at 0.46 nm and the Au volume increase entirely contributes to develop the ⟨001⟩ pyramids. The stabilization at 0.46 nm (two MLs) of h^{Au}_{111} is a strong indication that h^{Au}_{111} is driven by the wetting of Au on {110} Fe. This is indeed the critical thickness chosen in Sec. II E 2 (Fig. 4). To verify this hypothesis, we modified this critical thickness and we found that effectively this value directly monitors h^{Au}_{111} of the M2 minima.

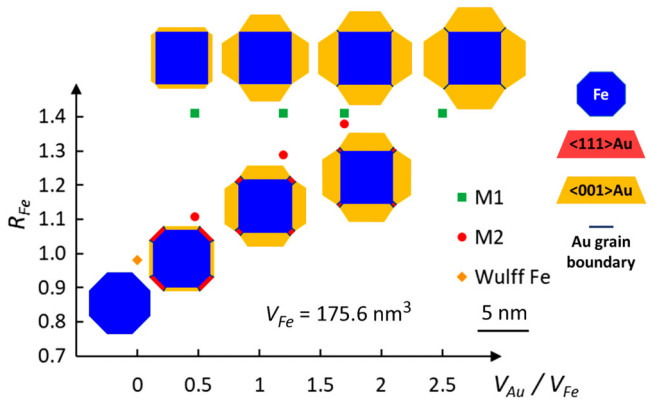

FIG. 11. Optimal shapes illustrated for $V_{Au}/V_{Fe} = 0$, 0.47, 1.2, 1.7, and 2.5 volume ratios. The shapes are at the scale for $V_{Fe} = 175.6$ nm^3.

To summarize, the M2 minimum progressively evolves from a shape purely driven by the wetting (for $V_{Au}/V_{Fe} = 0.47$) to an intermediate shape driven by the combination of the wetting for {111}Au on {110}Fe, the interface optimization, and the formation of ⟨001⟩ oriented Au pyramids (the 3D SK-like growth mode), as illustrated in Fig. 11 (red points). Around the volume ratio 1.7, the M2 minimum disappears and the M1 minimum only subsists.

C. Shape evolution with the volume ratio and comparison with experimental NPs

We now discuss which shape is the most likely to develop as a function of the volume ratio, assuming that the growth conditions allow us to reach one of the two optimal shapes (M1 or M2 minimum) at each step, as reported in Fig. 11. For $V_{Fe} = 175.6$ nm^3, $V_{Au}/V_{Fe} = 0.47$ is the minimal ratio ensuring a full wetting with two MLs. The M2 minimum can thus be given by Eq. (29) for $f = 1$ and is $R^{homo}_{Fe} = 1.11$. As the latter value is by chance close to $R^{Wulff}_{Fe} = 0.98$ corresponding to the Wulff shape of bare iron (yellow point in Fig. 11), M2 can be easily achieved. Although M1 has a lower energy than M2, the barrier $\Delta E_{M2 \to SP}$ from M2 to the saddle point SP is so high (10^{-17} J from Fig. 12, i.e., 60 eV) that it prevents the M2 to M1 transition. (In addition, the physical meaning of M1 is questionable for low volume ratios. Indeed, our geometrical model does not correctly ensure the full wetting at the core corners below $V_{Fe} = 1.2$.)

The barrier $\Delta E_{M2 \to SP}$ decreases from 10^{-17} J (or 60 eV) for $V_{Au}/V_{Fe} = 0.47$ to zero for V_{Au}/V_{Fe} close to 1.7 (Fig. 12). When it is sufficiently low, a shape transition from M2 to M1 will occur, at the latest for $V_{Au}/V_{Fe} = 1.7$ (Fig. 11). Once the M1 shape is reached, the NP shell will continue to grow with the optimal

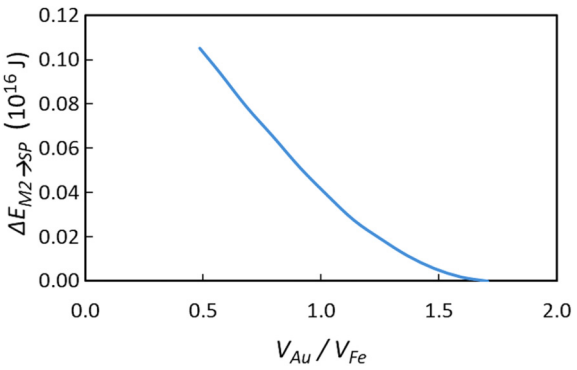

FIG. 12. Energy barrier $\Delta E_{M2\to SP}$ separating the M2 minimum and the saddle point SP (for $V_{Fe} = 175.6$ nm^3).

truncation $t_{opt} = 0.534$ that reflects an optimal distribution of the areas of the {111}Au and {001}Au surfaces within our model.

Note that the M1 shapes are not sensitive to changes in the interface energy densities, providing that their ratio is larger than $\sqrt{2}$. The details of the M2 shapes are sensitive to these parameters and to the critical thicknesses chosen for Au wetting. The relative hierarchy of M1 and M2 and the barrier between them (position of the SP) also depend on these parameters. However, the scenarios described in Figs. 8, 9, and 11 are unchanged.

These morphologies are in excellent agreement with those experimentally observed.

In Ref. 7 (and in its supplemental material), one collection of bare Fe NPs and two different collections of Fe–Au NPs were achieved with the same size distribution of core and similar relative size dispersions before and after gold deposit. As the Fe volume explored in detail here was chosen to fit the mean experimental core size, a direct comparison with the shapes predicted in Figs. 7, 9, and 11 is possible.

The NP in Fig. 1(b) and those from the same collection in Ref. 7 present a polyhedral shape with an octagonal section and a full coverage of about two or three Au MLs, which is completely accounted for by the M2 minimum predicted for low volume ratio.

Regarding the NPs from the second collection reported in Ref. 7 (and from Ref. 9), most of them present a core shape close to a cube and well-formed pyramids, as displayed in Fig. 1(a), and an experimental Au/Fe volume ratio estimated in the range of 1.6–2.3. The {111}Au/{110}Fe interfaces barely even exist and the core corners are covered by two or more Au MLs. Moreover, homogeneous thickness or octagonal sections are not observed when the Au/Fe volume ratio is in this range. The observed NPs are thus very well reproduced by the M2 minimum shortly before the M2 to M1 shape transition. In addition, we compare in Fig. 13 the predicted optimal truncation and the experimental truncations measured in 20 pyramids from five NPs (TEM observations in ⟨001⟩Fe zone axis allow us to explore four of the six pyramids of a NP). Given the error bars, we estimate the below:

(i) About 30% of observed pyramids have reached the calculated optimal truncation ($t \sim t_{opt}$).

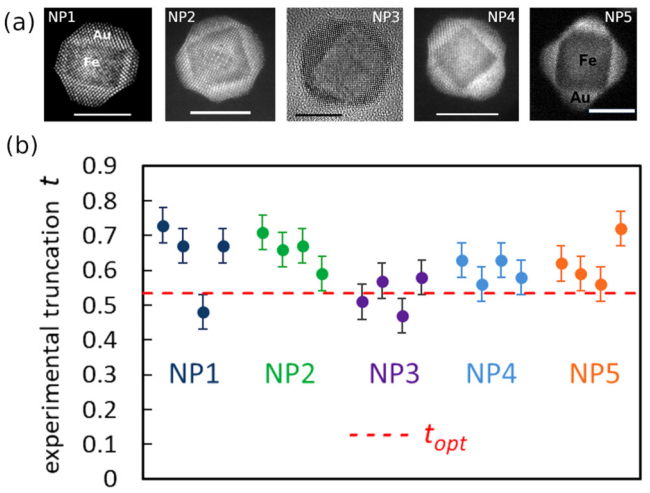

FIG. 13. (a) TEM images (the scale bars are 5 nm) and (b) experimental truncations t in five different NPs with well-formed pyramids, measured from the TEM images. The dashed line is the optimal truncation (0.534) predicted by the model for large Au/Fe volume ratio.

(ii) About 60% are more truncated ($t > t_{opt}$).
(iii) Only 10% pyramids are slightly less truncated ($t < t_{opt}$).

So, the experimental observations are very consistent with our model, where pyramids flatter than the optimal shape can exist due to an insufficient amount of gold, but sharper pyramids cannot form.

To conclude, the comparison of the experimental NPs with the predictions of the model indicates that most of them are close to their individual equilibrium shape, given the core size and the available gold amount.

D. Impact of the iron volume V_{Fe} on the optimal shape

Let us briefly discuss the role of the core size.

(i) As long as the surface and interface energy densities do not depend on Au thickness, i.e., as long as the Au thicknesses are larger than the critical thicknesses defined in Sec. II E 2 (Fig. 4), the NP energy as displayed in Figs. 6 and 7 scales with $(V_{Fe})^{2/3}$. A universal function $E_{NP}/(V_{Fe})^{2/3}$ could be used to describe the NP energy, reducing the number of geometrical parameters to 3: f, R_{Fe}, and V_{Au}/V_{Fe}. This quantity is homogeneous to a surface energy density. A consequence is that the M1 minimum shape is regardless of the core volume.

(ii) The change due to the thinness of the Au shell below two MLs depends also on $(V_{Fe})^{1/3}$, so that the core size impacts the M2 minimum. Figure 14 displays the core shape of the M2 minimum as a function of V_{Au}/V_{Fe} for the reference volume $V_{Fe} = 175.6$ nm^3, a volume 8 times smaller, and a volume 512 times larger (red, blue, and yellow curves, respectively). The M2 minimum disappears more quickly with V_{Au}/V_{Fe} for large

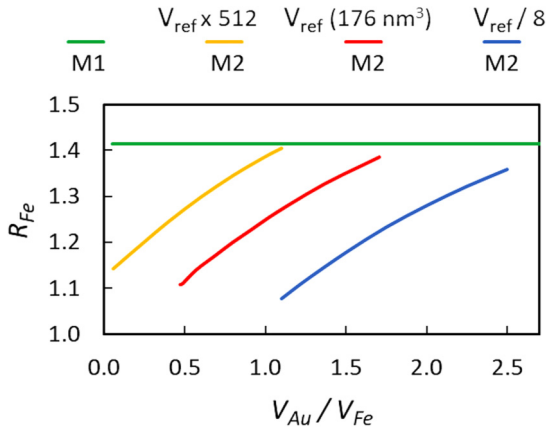

FIG. 14. Core shape R_{Fe} of the optimal shapes as a function of the Au/Fe volume ratio for various iron volumes. The red curve is for the reference volume $V_{Fe} = 175.6\ nm^3$, the blue curve is for a volume 8 times smaller, and the yellow curve is for a volume 512 times larger (the core edges when the shape is a cube being 5.6 nm, 2.8 nm, and 44.8 nm, respectively). The onset of each M2 curve is for the full wetting of the core by two Au MLs.

V_{Fe} than for small V_{Fe}. For a same V_{Au}/V_{Fe}, R_{Fe} of the M2 minimum is closer to $\sqrt{2}$ for a large V_{Fe} than for small V_{Fe}. The last remark could explain the observations of almost cube-shaped Fe[10] or FeCo[11] cores for smaller volume ratios than discussed above. In these two references, the core sizes were significantly larger than in our particles.

E. Other driving forces (elastic energy and grain boundary energy)

Finally, we briefly discuss the possible roles of elastic energy and Au grain boundary energy, which are not included in our model.

Elastic energy in ⟨001⟩Au grains is due to the moderate misfit (0.6%) resulting from the rotation of the Au and Fe lattices at the {001}Au/{001}Fe interfaces. In ⟨111⟩Au grains, this 0.6% misfit exists in the ⟨110⟩Au//⟨001⟩Fe direction, and a residual misfit could subsist in the ⟨−112⟩Au//⟨110⟩Fe direction after relaxation through misfit dislocations. In a (001) 2D Au layer with a 0.6% misfit, the elastic energy is $2.8 \times 10^6\ J/m^3$,[9] and we estimated by the finite element method that it can be reduced by more than 50% thanks to the pyramidal shape.[9,28] For the small Au volumes discussed in Figs. 8 and 9, the gain in elastic energy provided by the pyramids is thus 2 orders of magnitude smaller than $\Delta E_{M2 \rightarrow SP}$. So the relaxation of elastic energy also favors pyramids and slightly reduces the volume ratio for which the barrier separating M2 and M1 is null or can be crossed, but it plays a very minor role compared to surface and interface optimization.

Regarding the grain boundaries in Au, their areas and thus the associated crystalline disorder are reduced in our model thanks to the constraint on the shell to adopt the same shape as the core (a shape divergence would increase the grain boundaries areas). The formation of six pyramidal grains at the detriment of the homothetic shell also reduces the boundary areas and thus their energetic costs. So, this additional driving force should also contribute to favor the formation of pyramids.

VI. CONCLUSION

Fe–Au NPs achieved through an ultrahigh vacuum growth process present a crystalline Fe core embedded in a polycrystalline Au shell, with core and shell morphologies both depending on the Au/Fe volume ratio.

First, the growth mode of a shell on a nanocrystal was discussed. If, for given surface and interface energy densities, a layer on a 2D infinite substrate follows the classical 2D Franck–van der Merve growth mode (full wetting), another growth mode takes place due to the finite size of the core. It presents some analogies with the Stranski–Krastanov growth mode (increase of the wetting factor with the deposited amount).

To elucidate the various morphologies of the observed NPs, the excess energy of the NPs compared to the same Au and Fe amounts in their bulk phases was calculated using a geometrical model. The energy densities of the surfaces and of the two possible Au/Fe interfaces were computed by DFT. The shapes that minimize the excess energy were determined as a function of the Au/Fe volume ratio from 0.47 to 2.5.

On the basis of the observed morphologies, our model provides two shape transformations that can modify the excess energy at constant Au and Fe volumes: (i) the transformation of the core, a regular polyhedron that can adopt any intermediate shape from a {110}Fe rhombohedral dodecahedron to a perfect {001}Fe cube; and (ii) the thickness modulation of the shell, through the formation of Au pyramids with a variable truncation rate.

Three different driving forces were identified: (i) the very strong wetting of Au on Fe that tends to preserve a minimal Au layer of about two MLs on each Fe core face. (ii) The interface energy minimization that favors the cube-shaped core. This is due to the ratio $\gamma^{interf}_{(111)Au/(110)Fe}/\gamma^{interf}_{(001)Au/(001)Fe}$ larger than $\sqrt{2}$ (about 1.8 from our DFT calculations). (iii) The minimization of Au surface energy, that can promote a 3D Stranski–Krastanov-like growth mode of Au on a Fe nanosubstrate. They can compete or cooperate depending on the Au/Fe volume ratio.

For large Au/Fe volume ratios, there is no competition between the three driving forces, and the two shape transformations cooperate so that the equilibrium shape cumulates the full wetting, the cube-shaped Fe core $\left(R_{Fe} = \sqrt{2}\right)$ that minimizes the interface energy and the Au pyramids that minimize the surface energy. From a volume ratio of 1.2, the pyramid truncation is stabilized at 0.535. This optimal theoretical truncation is in excellent agreement with the experimental observations.

For small Au/Fe volume ratio, another optimal shape with an octagonal section and a quasi-homogeneous Au shell thickness is favored. It is mainly driven by the full wetting of the iron core by gold. When the Au/Fe volume ratio just allows the coverage of Fe by two Au MLs, the shape is calculated by the Wulff theorem, considering on each core face the sum of the interface energy and Au surface energy [Eq. (29)]. For the Fe volume of $175.6\ nm^3$ (same order of magnitude as the experimental volumes), this volume ratio

is 0.47 and the core aspect ratio calculated is then $R_{Fe} = 1.11$. This calculated shape is very close to experimental NPs with an octagonal section as in Fig. 1(b) (observed R_{Fe} around 1 and a coverage of about 2.5 MLs).

Between these two extreme shapes, the wetting can be fully preserved, and the optimal shape progressively evolves with the Au/Fe volume ratio by the concomitant development of the Au pyramids and the transformation of the polyhedral core toward a cube.

The comparison of experimental Fe–Au NPs with the predictions of the model indicates that most of them are close to their individual equilibrium shape, given the core size and the available gold amount.

This analysis can be extended to other systems, including those where the epitaxial accommodation of two different crystalline systems result in NPs with a crystalline core and a polycrystalline shell, where it can provide a rational tool for predicting the NP equilibrium shapes and thus be helpful in mastering the shape dependent physical properties.

ACKNOWLEDGMENTS

The authors thank Nicolas Combe for critical reading of the manuscript and fruitful comments. This study has been (partially) supported through NEXT [Grant No. ANR-10-LABX-0037 (FUN)] in the framework of the "Programme des Investissements d'Avenir." DFT calculations were performed using HPC resources from CALMIP (Grant No. 2019-p1149).

APPENDIX A: CORE GEOMETRY

Figure 15(a) displays the (001)Fe cross section of the core, built by applying Eq. (1). A {001}Fe face is a square with the edge

$$b_{001}^{Fe} = 2\left(\sqrt{2}\,h_{110}^{Fe} - h_{001}^{Fe}\right) = 2\,h_{001}^{Fe}\left(\sqrt{2}\,R_{Fe} - 1\right). \quad \text{(A1)}$$

Figure 15(b) displays a {110}Fe face, an hexagon with the width

$$b_{110}^{Fe} = \sqrt{2}\left(2\,h_{001}^{Fe} - \sqrt{2}\,h_{110}^{Fe}\right) = 2\,h_{001}^{Fe}\left(\sqrt{2} - R_{Fe}\right). \quad \text{(A2)}$$

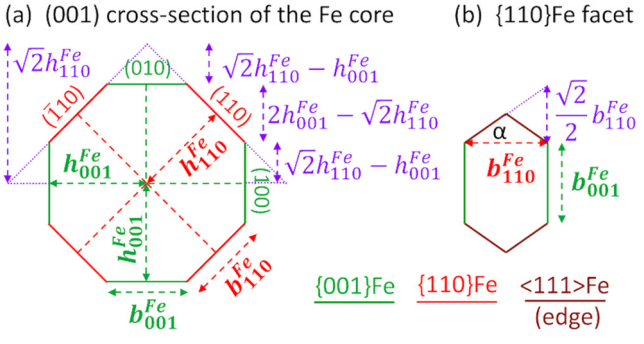

FIG. 15. Cross section (a) and {110} facet (b) of the core.

The angle α between the ⟨011⟩ and ⟨111⟩ edges of a {110}Fe face is 35.26° $(\cos\alpha = \sqrt{2}/\sqrt{3})$.

APPENDIX B: GEOMETRICAL LIMITS OF THE SHELL FOR A GIVEN CORE SHAPE R_{Fe}

The maximum values of f and t, f_{max} and t_{max}, depend only on V_{Au}/V_{Fe}. They are reached when the pyramids are empty ($V_{Au}^{pyr} = 0$ and $V_{Au} = V_{Au}^{homo}$). From Eq. (8), it becomes

$$f_{max} = (1 + V_{Au}/V_{Fe})^{1/3}; \quad t_{max} = 1, \quad \text{(B1)}$$

$$h_{pyr}^{Au} = 0 \text{ and } h_{111\_max}^{Au} = h_{110}^{Fe}\,(f_{max} - 1). \quad \text{(B2)}$$

The minimal values f_{min} and t_{min} result from the progressive building of the pyramids from the above situation. For a given R_{Fe}, there exists a threshold volume ratio $(V_{Au}/V_{Fe})_{th}$ for which $f = 1$ and $t = 0$ arise simultaneously so that $V_{Au} = 6\,V_{Au}^{pyr}$. It comes from Eqs. (6), (7), and (12),

$$\left(\frac{V_{Au}}{V_{Fe}}\right)_{th} = \frac{\sqrt{2}\,(S_{001}^{Fe})^{3/2}}{V_{Fe}} = \frac{2\,\left(\sqrt{2}\,R_{Fe} - 1\right)^3}{\sqrt{2} - 3\,R_{Fe}\left(\sqrt{2} - R_{Fe}\right)^2}. \quad \text{(B3)}$$

There are three possibilities:

(i) If $(V_{Au}/V_{Fe}) > (V_{Au}/V_{Fe})_{th}$: the homothetic shell subsists when the pyramids are complete so that $t_{min} = 0$. From Eqs. (7), (8), (12), and (B3), it becomes

$$f_{min} = \left(\frac{V_{Au} + V_{Fe}}{V_{Fe} + \sqrt{2}\,S_{001}^{Fe\ 3/2}}\right)^{1/3} = \left[\frac{1 + (V_{Au}/V_{Fe})}{1 + (V_{Au}/V_{Fe})_{th}}\right]^{1/3}, \quad \text{(B4)}$$

$$h_{111\_min}^{Au} = h_{110}^{Fe}\,(f_{min} - 1). \quad \text{(B5)}$$

(ii) If $(V_{Au}/V_{Fe}) = (V_{Au}/V_{Fe})_{th}$: the homothetic shell is empty and the pyramids are complete simultaneously so that $f_{min} = 1$ and $t_{min} = 0$.

(iii) If $(V_{Au}/V_{Fe}) < (V_{Au}/V_{Fe})_{th}$: then $f_{min} = 1$ because the homothetic shell is empty before the pyramids can be complete. In this situation, $h_{111\_min}^{Au} = h_{100\_min}^{Au} = 0$ and $V_{Au}^{pyr} = V_{Au}/6$. From Eqs. (12) and (B3) the minimal truncation is

$$t_{min} = \left(1 - \frac{V_{Au}}{\sqrt{2}\,S_{001}^{Fe\ 3/2}}\right)^{1/3} = \left[1 - \frac{(V_{Au}/V_{Fe})}{(V_{Au}/V_{Fe})_{th}}\right]^{1/3}. \quad \text{(B6)}$$

DATA AVAILABILITY

The data that support the findings of this study are available from the corresponding author upon reasonable request.

REFERENCES

[1] R. Ferrando, J. Jellinek, and R. L. Johnston, Chem. Rev. **108**, 845 (2008).

[2]D. Ferrer, A. Torres-Castro, X. Gao, S. Sepulveda-Guzman, U. Ortiz-Mendez, and M. Jose-Yacaman, Nano Lett. **7**, 1701 (2007).
[3]L. Piccolo, Z. Y. Li, I. Demiroglu, F. Moyon, Z. Konuspayeva, G. Berhault, P. Afanasiev, W. Lefebvre, J. Yuan, and R. L. Johnston, Sci. Rep. **6**, 35226 (2016).
[4]P. Chen, K. Murugappan, and M. R. Castell, Phys. Chem. Chem. Phys. **22**, 4416 (2020).
[5]D. Bochicchio and R. Ferrando, Phys. Rev. B **87**, 165435 (2013).
[6]C. Langlois, Z. L. Li, J. Yuan, D. Alloyeau, J. Nelayah, D. Bochicchio, R. Ferrando, and C. Ricolleau, Nanoscale **4**, 3381 (2012).
[7]P. Benzo, S. Combettes, B. Pecassou, N. Combe, M. Benoit, M. Respaud, and M. J. Casanove, Phys. Rev. Mater. **3**, 096001 (2019).
[8]A. Ponchet, L. Pedesseau, A. Le Corre, C. Cornet, and N. Bertru, Appl. Phys. Lett. **114**, 173102 (2019).
[9]C. Langlois, P. Benzo, R. Arenal, M. Benoit, J. Nicolai, N. Combe, A. Ponchet, and M. J. Casanove, Nano Lett. **15**, 5075 (2015).
[10]M. Kamp, A. Tymoczko, U. Schürmann, J. Jakobi, C. Rehbock, K. Rätzke, S. Barcikowski, and L. Kienle, Cryst. Growth Des. **18**, 5434 (2018).
[11]Y.-H. Xu and J.-P. Wang, Appl. Phys. Lett. **91**, 233107 (2007).
[12]H. Okamoto, T, B. Massalski, L. J. Swartzendruber, and P. A. Beck, Bull. Alloy Phase Diagrams **5**, 592 (1984).
[13]E. Bauer and J. H. van der Merwe, Phys. Rev. B **33**, 3657 (1986).
[14]H. F. Jurca, A. Damian, C. Gougaud, D. Thiaudière, R. Cortès, F. Maroun, and P. Allongue, J. Phys. Chem. C **120**, 16080 (2016).
[15]J. Wang and S.-Q. Wang, Surf. Sci. **630**, 216 (2014).
[16]L. Vitos, A. Ruban, H. Skriver, and J. Kollár, Surf. Sci. **411**, 186 (1998).
[17]Y. Saito, J. Cryst. Growth **53**, 273 (1981).
[18]R. Tran, Z. Xu, B. Radhakrishnan *et al.*, Sci. Data **3**, 160080 (2016).
[19]M. Nicholas, J. Mater. Sci. **3**, 571 (1968).
[20]M. Benoit, C. Langlois, N. Combe, H. Tang, and M.-J. Casanove, Phys. Rev. B **86**, 075460 (2012).
[21]M. Benoit, N. Combe, A. Ponchet, J. Morillo, and M.-J. Casanove, Phys. Rev. B **90**, 165437 (2014).
[22]S. Giorgio, C. Chapon, C. R. Henry, G. Nihoul, and J. M. Penisson, Ultramiscrocopy **38**, 1 (1991).
[23]W. R. Miller and W. A. Tyson, Surf. Sci. **62**, 267 (1977).
[24]S. Lu, Q. M. Hu, M. P. J. Punkkinen, B. Johansson, and L. Vitos, Phys. Rev. B **87**, 224104 (2013).
[25]D. Amram and E. Rabkin, ACS Nano **8**, 10687 (2014).
[26]P. Müller and R. Kern, Appl. Surf. Sci. **102**, 6 (1996).
[27]J. Tersoff and F. K. LeGoues, Phys. Rev. Lett. **72**, 3570 (1994).
[28]A. Ponchet, D. Lacombe, L. Durand, D. Alquier, and J.-M. Cardonna, Appl. Phys. Lett. **72**, 2984 (1998).
[29]Note that Fig. 5 is presented regardless the NP size. However, this is valid only when the Au thickness is larger than the critical thickness defined in Sec. II E 2 for the full wetting condition. For instance, for the 175.6 nm^3 V_{Fe} discussed in Sec. IV, and R_{Fe} around 1, Fig. 5 is valid for V_{Au}/V_{Fe} larger than 0.47 if the critical thickness is two MLs.
[30]There, however, exists a particular volume ratio where the 3D wetting factor $\Phi_{Au/(3D)Fe}$ is identical whatever R_{Fe} and its hierarchy as a function of R_{Fe} undergoes an inversion. It is given from (15) and (23) by $V_{Au}/V_{Fe} = [1 + (\Phi_{(001)Au/(001)Fe} - \Phi_{(111)Au/(110)Fe})/(\gamma^{Au}_{111} - \gamma^{Au}_{001})]^{3/2} - 1$ and is 3.4 here. For lower volume ratios, the larger the predefined R_{Fe} of the core [i.e., the larger the (001)Au/(001)Fe interface area], the larger the energetic benefit to form a shell homothetic to the core as shown by the smaller $\Phi_{Au/(3D)Fe}$. This is because of the hierarchy of the 2D wetting factors ($\Phi_{(111)Au/(110)Fe} > \Phi_{(001)Au/(001)Fe}$). As the volume ratio increases, the surface term in the shell formation energy ΔF becomes dominant. As $\gamma^{Au}_{111} < \gamma^{Au}_{001}$, the cost to form a shell becomes larger ($\Phi_{Au/(3D)Fe}$ becomes larger) with large R_{Fe} than with small R_{Fe}. If ($\Phi_{(001)Au/(001)Fe} - \Phi_{(111)Au/(110)Fe}$) and ($\gamma^{Au}_{111} - \gamma^{Au}_{001}$) had the opposite sign, this inversion would not exist.